Prediction of Mining-Induced Subsidence in Saudi Arabia Phosphate Mines Using ANN Method

Atef GHARBI[1], Mohamed AYARI[2], Yamen El Touati[3],
Zeineb Klai[4], Mahmoud Salaheldin Elsayed[5], Elsaid Md. Abdelrahim[6]
Department of Information Systems-Faculty of Computing and Information Technology,
Northern Border University, Rafha 91911, Saudi Arabia[1]
Department of Information Technology-Faculty of Computing and Information Technology,
Northern Border University, Rafha 91911, Saudi Arabia[2]
Department of Computer Sciences-Faculty of Computing and Information Technology,
Northern Border University, Rafha, Saudi Arabia[3, 4, 5]
Computer Science Department-Science College, Northern Border University (NBU), Arar 73213, Saudi Arabia[6]

***Abstract*—This study develops and validates an artificial neural network (ANN) model to predict mining-induced land subsidence in Saudi Arabia's Al-Jalamid and Umm Wu'al phosphate mines. A multilayer perceptron is used with optimized hyperparameters based on four inputs (ground point position, distance from extraction center, accumulated exploitation volume, and time). The optimal configuration (5 hidden layers, 64 nodes, 240 epochs) achieves RMSE = 22 mm and MAE = 13 mm, outperforming traditional numerical/statistical baselines. Case-study validation at both mines confirms robustness (e.g., RMSE ≈ 20 mm, MAE ≈ 12 mm), enabling practical mitigation such as ground reinforcement and extraction-rate control. The results demonstrate that a tuned ANN provides accurate, operationally useful subsidence forecasts, supporting safer and more sustainable mine planning.**

Keywords*—Subsidence prediction; phosphate mine; artificial neural network; multilayer perceptron; hyperparameter optimization

I. Introduction

Phosphate mining is a cornerstone of Saudi Arabia's mining industry, playing a pivotal role in the nation's economic development. As one of the world's largest producers of phosphate, Saudi Arabia contributes significantly to global fertilizer production, which is essential for sustaining agricultural productivity and food security. The Al-Jalamid and Umm Wu'al phosphate mines, located in the Northern Borders Province, are among the most significant reserves globally, with extensive deposits that support both domestic and international demand. However, the extraction of phosphate is not without its challenges. Mining activities, particularly underground operations, often lead to environmental and geological disturbances, with land subsidence being one of the most critical issues. Subsidence can result in the sinking or settling of the ground surface, leading to infrastructure damage, environmental degradation, and increased operational risks. These impacts are exacerbated in arid regions like Saudi Arabia, where the geological formations are susceptible to deformation due to mining activities.

Mining-induced subsidence poses significant risks to both the environment and infrastructure. In Saudi Arabian phosphate mines, the extraction of phosphate-rich layers disrupts the geological equilibrium, causing the overlying strata to collapse or settle. This subsidence can lead to the formation of sinkholes, cracks in the ground surface, and damage to nearby infrastructure such as roads, pipelines, and buildings. Additionally, subsidence can alter groundwater flow patterns, further exacerbating environmental concerns in a region already facing water scarcity. Accurate prediction of subsidence is therefore essential for mitigating these risks, enabling mine operators to implement preventive measures, optimize extraction processes, and ensure the safety and sustainability of mining operations. Despite advancements in predictive modeling, the complex interplay of geological, hydrological, and operational factors makes subsidence prediction a challenging task, necessitating the development of robust and reliable models.

Over the past decade, various methodologies have been proposed to predict mining-induced subsidence, ranging from traditional numerical: [1] analyzed land subsidence using monitoring and numerical simulation in linear engineering areas, [2] modeled surface subsidence in coal mines through a bonded block numerical method, and [3] examined the geotechnical characterization of phosphate mining waste materials for pavement applications. Furthermore, [4] compared statistical and machine learning approaches for land subsidence modelling, [5] proposed a novel prediction method using data assimilation techniques, and [6] introduced a probability integral model integrated with active and passive remote sensing data to monitor subsidence. Numerical methods, such as the two-dimensional seepage model, quasi-three-dimensional seepage model, and fully coupled three-dimensional method, offer relatively straightforward implementation and interpretation [7-8]. While these methods provide detailed insights into subsidence mechanisms, they often require extensive computational resources and precise input parameters, limiting their practical applicability.

Statistical techniques, including time-series modeling [9-11], regression analysis [12-13], and Grey theory [14-16] offer simpler alternatives but are often constrained by their inability to capture the nonlinear relationships inherent in subsidence data.

Recent advancements in artificial intelligence (AI) have revolutionized subsidence prediction, with machine learning models such as Support Vector Machines (SVMs) and Artificial Neural Networks (ANNs) demonstrating superior performance. SVMs, known for their ability to handle high-dimensional data, have been successfully applied in subsidence prediction, particularly in cases with limited datasets [17-18]. However, their scalability remains a concern for large-scale mining operations. ANNs, on the other hand, have gained prominence due to their ability to model complex, nonlinear relationships and adapt to diverse datasets [19-21]. Studies have highlighted the effectiveness of ANNs in predicting subsidence, particularly when integrated with remote sensing and geographic information system (GIS) data. Despite these advancements, there is a need for further research to optimize ANN architectures, improve prediction accuracy, and address the challenges associated with long-term subsidence forecasting. The ANN model can be used to predict subsidence at different locations and times, helping mine operators to minimize subsidence, implement mitigation measures to protect infrastructure and the environment, monitor subsidence trends over time.

Despite various numerical and statistical models for subsidence prediction, their applicability is often limited by computational constraints and the complexity of subsurface interactions. Traditional methods struggle to account for nonlinear geological behaviors, making them unsuitable for large-scale, real-time applications. This study aims to address this gap by developing an ANN model tailored to the unique geological and operational conditions of Saudi Arabian phosphate mines offering a robust alternative for subsidence prediction.

By leveraging advanced machine learning techniques, the proposed model seeks to provide accurate and reliable subsidence predictions, contributing to the sustainable management of mining operations and the mitigation of environmental risks.

This study presents an artificial neural network (ANN) model for predicting mining-induced subsidence in Saudi Arabian phosphate mines. The paper is structured as follows: Section II provides an overview of the study area, including geological characteristics and mining conditions. Section III details the methodology, describing the ANN model architecture, feature selection, and training process. Section IV presents the results, including model performance evaluation and validation. Finally, Section V concludes the study with key insights and recommendations for future research.

II. Study Area

As two of the world's largest phosphate reserves, the Al-Jalamid and Umm Wu'al mines in Saudi Arabia's Northern Borders Province possess unique geological and economic significance. Their sedimentary formations, characterized by alternating limestone, shale, and phosphorite layers, make them highly susceptible to subsidence. Previous studies have reported significant subsidence events in these mines, highlighting the need for advanced predictive models. The presence of Tunnel Boring Machines (TBMs) further complicates ground stability, making these sites ideal for testing AI-driven predictive frameworks.

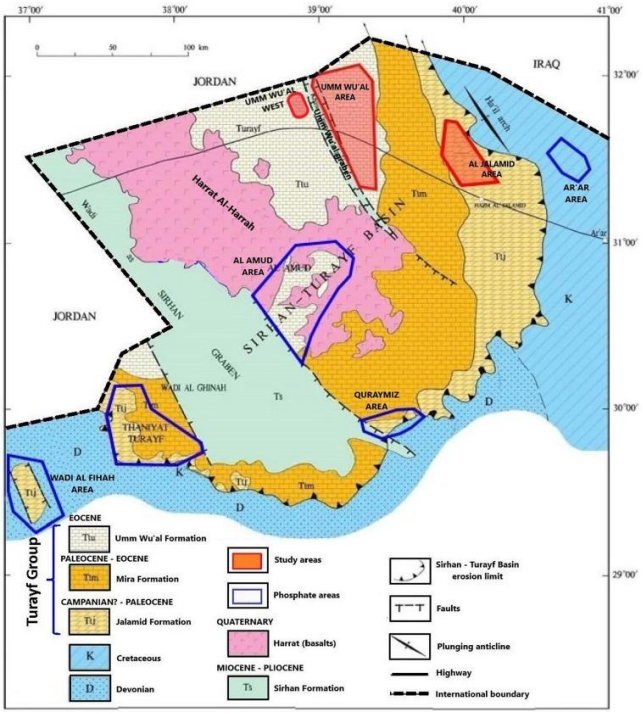

Fig. 1. Geological framework of the sirhan-turayf basin: distribution of phosphate deposits and study sites.

Fig. 1 presents the Al-Jalamid and Umm Wu'al phosphate mines in northern Saudi Arabia, among the world's largest phosphate reserves, crucial for global fertilizer production. Al-Jalamid is a major underground mining site where extraction has led to land subsidence and high disc cutter consumption in TBMs. The region's sedimentary formations (limestone, shale, phosphate-rich layers) present geological and environmental challenges due to its arid climate and limited groundwater.

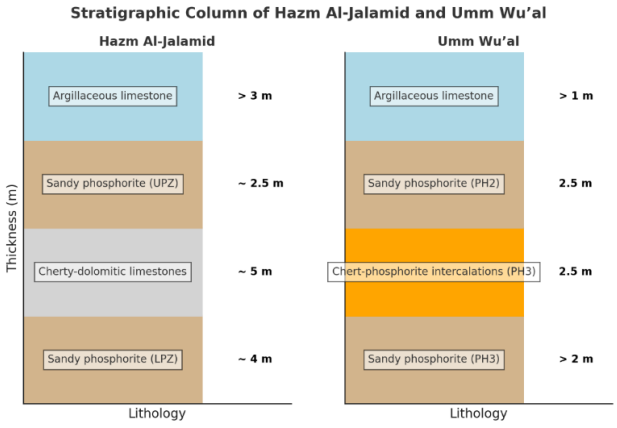

Fig. 2. Stratigraphic columns of phosphate-bearing formations in Hazm Al-Jalamid and Umm Wu'al.

Fig. 2 introduces the phosphorite deposits at Hazm Al-Jalamid range from friable sandy-calcareous to hard compact formations, reflecting depositional and diagenetic variations that influence mining methods and geotechnical behavior. The

Thaniyat Phosphorite Member comprises two main phosphorite horizons: Lower Phosphorite Zone (LPZ) and Upper Phosphorite Zone (UPZ).

The LPZ consists of calcareous and dolomitic phosphorite beds (3–4 m thick), rich in bioclastic fragments, indicating a marine depositional environment. The UPZ, 4–7 m thick (avg. 6 m), contains sparry calcite lenses, argillaceous cement, and vuggy structures, suggesting post-depositional diagenesis and bioturbation. A 12-meter-thick sand, clay, and limestone sequence overlies the UPZ.

An intermediate horizon (0.5–5 m thick) between LPZ and UPZ consists of low-grade phosphatic dolomitic limestone with quartz geodes and chert nodules, marking a transitional depositional setting influenced by sedimentological and chemical variations.

III. Artificial Neural Networks

The dataset employed in this study was collected from monitoring records of the Al-Jalamid and Umm Wu'al phosphate mines located in the Northern Borders Province of Saudi Arabia. It consists of ground deformation measurements covering multiple observation points distributed across subsidence-prone areas. Four primary variables were included: (i) ground point positions (Y), representing the spatial coordinates of monitoring stations along the subsidence trough; (ii) distance from the extraction chamber center (L), indicating the horizontal offset of each point from the center of mining activity; (iii) accumulated exploitation volume (V), defined as the total phosphate volume extracted up to a given measurement epoch; and (iv) time (T), denoting the elapsed duration since the initiation of mining operations.

The dataset underwent several preprocessing steps to ensure consistency and reliability. Missing values were handled using linear interpolation for continuous features, while outliers were identified and removed. All input features were normalized to a [0, 1] range to eliminate scale differences and enhance model convergence. Following preprocessing, the dataset was divided into three subsets: 70% for training the artificial neural network (ANN), 15% for hyperparameter validation, and 15% for final performance testing. This partitioning ensured robust evaluation and reduced overfitting risks.

A. Artificial Neural Network Architecture

Fig. 3 presents the proposed ANN model is designed to predict mining-induced subsidence using a multilayer perceptron (MLP) architecture. The model consists of three primary components: an input layer, hidden layers, and an output layer.

1) Input layer: The input layer comprises four neurons, each corresponding to one of the input variables:

a) Ground point positions (Y): The spatial coordinates of monitoring points along the subsidence trough.

b) Distance from extraction chamber center (L): The horizontal distance from the center of the mining activity to each monitoring point.

c) Accumulated exploitation volume (V): The total volume of phosphate extracted up to the measurement epoch.

d) Time (T): The elapsed time since the start of mining operations.

2) Hidden layers: The model includes two hidden layers, each containing 64 neurons. The number of hidden layers and neurons was determined through validation, balancing model complexity and generalization performance. The Rectified Linear Unit (ReLU) activation function was used for the hidden layers, as it effectively mitigates the vanishing gradient problem and accelerates convergence during training.

3) Output layer: The output layer consists of a single neuron that predicts the subsidence value (η). A sigmoid activation function was employed in the output layer to ensure that the predicted subsidence values fall within a realistic range (0 to 1, normalized to the maximum observed subsidence).

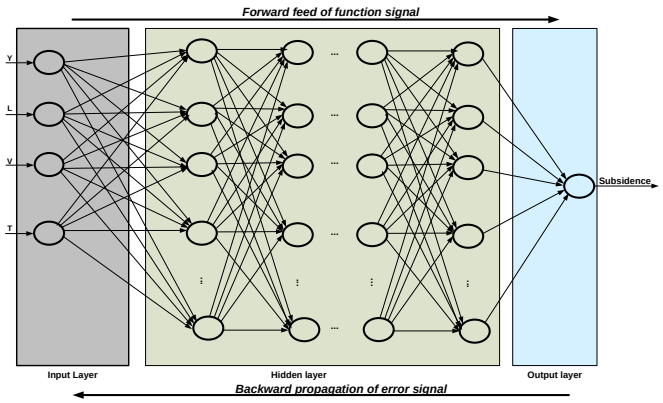

Fig. 3. Architecture of the Backpropagation Neural Network (BPNN) for subsidence prediction.

B. Data Preprocessing

The dataset used for training and testing the ANN model was preprocessed to ensure optimal performance. The preprocessing steps included as it is illustrated in Fig. 4:

1) Data cleaning: Missing values in the dataset were addressed using linear interpolation for continuous variables and mode imputation for categorical variables. Outliers were detected and eliminated from the dataset.

2) Normalization: All input variables were normalized to a range of [0, 1] using min-max scaling to ensure that features with larger magnitudes did not dominate the training process. The normalization formula is given by:

$$X_{norm}=(X-X_{min})/(X_{max}-X_{min})$$

where X_{min} and X_{max} are the minimum and maximum values of the feature, respectively.

3) Feature selection: A correlation analysis was conducted to identify and remove highly correlated features, reducing redundancy and improving model efficiency. The final set of features included ground point positions, distance

from the extraction chamber center, accumulated exploitation volume, and time.

4) Data splitting: To ensure rigorous model assessment, the data were split into three subsets: 70% for training the ANN, 15% for hyperparameter validation, and 15% for final performance testing.

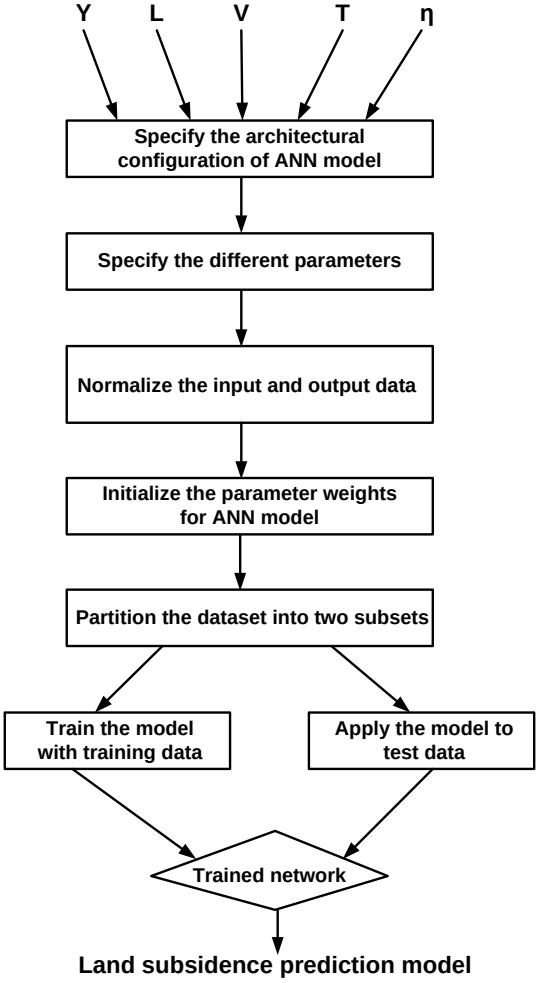

Fig. 4. Workflow of the ANN model for land subsidence prediction.

C. Model Training

In Artificial Neural Network (ANN) models, each neuron in the input layer receives an assigned input, which is transmitted to neurons in subsequent layers through weighted connections. These weights, ranging from -1 to 1, represent the relative importance of each connection. To determine the neuron's response, an activation function is applied to the weighted input, producing an output value. If this value exceeds a predefined threshold, the neuron becomes active; otherwise, it remains inactive.

In the output layer, the discrepancy between the predicted and actual output is quantified as an error. Through a process known as backpropagation, this error propagates backward through the network, adjusting the weights of preceding layers. This iterative process continues until the error converges below a specified threshold, optimizing the network's predictive accuracy.

Following the training phase, the validation and testing phases commence. During validation, hyperparameters such as training duration, learning rates, and the number of neurons in hidden layers are fine-tuned to enhance model performance. The testing phase assesses the model's generalization ability, evaluating its predictive accuracy on unseen data. The final model is selected based on its optimal performance metrics.

The GIS-integrated ANN framework utilized a backpropagation neural network (BPNN) for land subsidence susceptibility assessment, with performance evaluated via correlation coefficient. The training phase mathematics and convergence behavior are derived as follows:

The outputs of the hidden layer h_i and output layer O_k are given by Eq. (1) and Eq. (2).

$$h_i = F(V_j) = \left[B_{oj} + \sum_{i=1}^{I} (B_{ij} \cdot v_i) \right] \quad (1)$$

$$O_k = F(H_k) = \left[B_{ok} + \sum_{j=1}^{J} (B_{kj} \cdot h_i) \right] \quad (2)$$

where V_j and H_k denote the intermediate computations before activation; B_{oj} and B_{ok} correspond to bias terms that establish threshold values; F signifies the activation function operating within a range of 0 to 1; and v_i, h_i, and O_k refer to the input, hidden, and output layers, respectively.

For activation functions, the hyperbolic tangent sigmoid is used, which computes the outputs of hidden and output layers as given in Eq. (3) and Eq. (4).

$$h_i = F(V_j) = \frac{1}{1+e^{-V_j}} \quad (3)$$

$$O_k = F(H_k) = \frac{1}{1+e^{-H_k}} \quad (4)$$

The error function E is formulated as shown in Eq. (5).

$$E = \frac{1}{2} \sum_{k=1}^{K} O_k^2 = \frac{1}{2} \sum_{k=1}^{K} (d_k - O_k)^2 \quad (5)$$

Here, E represents the cumulative error across all output nodes, calculated as the sum of squared deviations between the network's predictions and target values. For each output node k, d_k denotes the desired target value, while ε_k corresponds to the prediction error (i.e., $\varepsilon_k = d_k - O_k$,). The weight modification between the hidden and output layers is defined as shown in Eq. (6).

$$\Delta b_{jk} = \alpha \cdot h_j \cdot \delta_k \quad (6)$$

where α is the learning rate. Reformulating Eq. (6) yields Eq. (7).

$$b_{jk}(n+1) = b_{jk}(n) + \Delta b_{jk}(n) \quad (7)$$

where n represents the iteration index. Taking the partial derivative of the error E with respect to b_{ij}, the following relations are derived:

The correlation coefficient (C) served as the primary performance metric for evaluating the GIS-integrated ANN model, it is calculated as shown in Eq. (8).

$$C=\frac{\sum_{i=1}^{n}(d_i-\bar{d})(p_i-\bar{p})}{\sqrt{\sum_{i=1}^{n}(d_i-\bar{d})^2\cdot\sum_{i=1}^{n}(p_i-\bar{p})^2}} \quad (8)$$

where C denotes the correlation coefficient, d_i is the target output, p_i is the predicted output, $\bar{d}$ is the mean target value, and $\bar{p}$ is the mean predicted output. Fig. 3 illustrates the architecture of the proposed predictive framework, which integrates a backpropagation neural network (BPNN) with four critical geospatial input parameters: (i) Percentage of agricultural land use, (ii) Energy consumption by groundwater extraction wells, (iii) Proportion of fine-grained sediments, and (iv) Mean maximum drainage path length.

Fig. 3 presents a comprehensive view of the primary stages in ANN configuration. While defining the network architecture, selecting activation functions, and determining the number of training epochs necessitate manual adjustments, automated processes manage data preprocessing, normalization, and weight initialization.

IV. Model Performance Evaluation

A. Performance Metrics

Multiple combinations of hyperparameters were tested, including:

- Number of hidden layers (e.g., 3, 4, 5, 6, …).
- Number of nodes per hidden layer (e.g., 32, 64, 128, …).
- Number of epochs (e.g., 100, 200, 240, 300, …).

Instead of using a grid search (testing all possible combinations), a random search is used (testing random combinations) to find the optimal hyperparameters. This approach was selected for the following reason. Random search explores the hyperparameter space more efficiently by sampling parameter combinations randomly, rather than exhaustively evaluating all possible combinations as in grid search. This is particularly advantageous when dealing with computationally expensive models.

For each combination of hyperparameters, the RMSE and MAE are recorded on the validation set and calculate the average RMSE and MAE for each hyperparameter combination.

The performance of the models was evaluated using:

- RMSE: Measures the average magnitude of the prediction errors.
- MAE: Provides a robust measure of error, less sensitive to outliers.

B. Optimal Hyperparameters

Table I presents a detailed summary of performance metrics corresponding to various artificial neural network (ANN) architectures. The "Hidden Layers" column denotes the number of hidden layers employed in each architecture, which directly affects the model's capacity to capture non-linear and complex data patterns. The "Hidden Nodes" column indicates the number of neurons per hidden layer; increasing this number generally enhances the model's representational power but may also heighten the risk of overfitting. The "Epochs" column specifies the total number of training iterations over the dataset, where a higher count may improve convergence but similarly raise overfitting concerns. The "Avg. RMSE (mm)" and "Avg. MAE (mm)" columns report the average root mean square error and mean absolute error, respectively, across validation folds—lower values in both metrics are indicative of better predictive performance. Finally, the "Std. Dev. RMSE" and "Std. Dev. MAE" columns reflect the standard deviations of RMSE and MAE, providing insight into the stability and consistency of each model's performance across k-fold cross-validation.

Insights from Table I reveal that as the number of hidden layers and nodes increases, the average RMSE and MAE generally decrease, suggesting that more complex architectures may yield better performance.

TABLE I. PERFORMANCE OF DIFFERENT ANN ARCHITECTURES

Hidden Layers	Hidden Nodes	Epochs	Avg. RMSE (mm)	Avg. MAE (mm)	Std. Dev. RMSE	Std. Dev. MAE
3	32	100	25.3	15.2	1.2	0.8
3	64	100	24.8	14.9	1.1	0.7
3	128	100	24.5	14.7	1.3	0.9
4	32	200	23.8	14.3	1	0.6
4	64	200	23.1	14	0.9	0.5
4	128	200	23.5	14.2	1.1	0.7
5	32	240	22.5	13.5	0.8	0.5
5	**64**	**240**	**22**	**13**	**0.7**	**0.4**
5	128	240	22.3	13.2	0.9	0.6
6	32	300	23	14.1	1	0.6
6	64	300	22.8	13.8	0.9	0.5
6	128	300	23.2	14	1.1	0.7

The bolded row (5 hidden layers, 64 hidden nodes, 240 epochs) represents the optimal configuration, as it achieves the lowest RMSE (22.0 mm) and lowest MAE (13.0 mm) with the smallest standard deviations (0.7 for RMSE and 0.4 for MAE). This configuration strikes a balance between model complexity and generalization, avoiding overfitting while maintaining high predictive accuracy.

Increasing the number of hidden layers beyond 5 does not significantly improve performance and may lead to overfitting, as seen in the 6-layer configurations. A moderate number of

hidden nodes (e.g., 64) provides the best balance between model complexity and performance, with fewer nodes (e.g., 32) resulting in higher errors and more nodes (e.g., 128) not yielding significant improvements. Training for 240 epochs is sufficient for convergence, as extending training to 300 epochs does not improve performance and may increase the risk of overfitting.

C. Case Studies

The ANN model was applied to two real-world case studies in Saudi Arabian phosphate mines to demonstrate its practical applicability:

1) Al-Jalamid mine: The model was used to predict subsidence in the Al-Jalamid mine, where extensive underground mining has led to significant ground deformation. The predictions were compared with actual subsidence measurements, achieving an RMSE of 20 mm and an MAE of 12 mm. The model's accuracy enabled mine operators to implement targeted mitigation measures, such as ground reinforcement and controlled extraction rates, reducing the risk of infrastructure damage.

2) Umm Wu'al mine: In the Umm Wu'al mine, the model was employed to forecast subsidence trends. The predictions were used to optimize mining operations, ensuring that subsidence remained within acceptable limits. The model's ability to provide long-term forecasts was particularly valuable for strategic planning and risk management.

V. Conclusions

This study developed an Artificial Neural Network (ANN) model to predict mining-induced subsidence in Saudi Arabian phosphate mines. The model demonstrated high predictive accuracy, achieving an RMSE of 22 mm, and an MAE of 13 mm, on the testing dataset. Key factors influencing subsidence, including distance from the extraction chamber center and accumulated exploitation volume, were identified through feature importance analysis. The model's robustness and adaptability make it a reliable tool for subsidence prediction in mining operations.

The proposed Artificial Neural Network (ANN) model offers significant practical benefits for the mining industry and environmental management. Risk mitigation is achieved through accurate subsidence prediction, allowing mine operators to implement targeted measures such as ground reinforcement and controlled extraction rates, thereby reducing the risk of infrastructure damage and environmental degradation. The model also enhances operational optimization by forecasting subsidence trends over time, ensuring mining activities remain within safe and sustainable limits. Additionally, it aids in strategic planning by providing long-term subsidence predictions, enabling mining companies to balance economic objectives with environmental and safety considerations. Furthermore, the model promotes environmental protection by minimizing subsidence-related impacts such as groundwater disruption and land deformation, which is particularly crucial in ecologically sensitive regions like Saudi Arabia.

Building upon the current findings, future research will aim to address the identified limitations and enhance the robustness and applicability of the ANN model. First, efforts will focus on integrating higher-resolution and more diverse ground truth datasets to reduce spatial bias and improve model generalization across heterogeneous regions. Second, to improve model interpretability, future studies will explore hybrid approaches that couple ANN models with explainable artificial intelligence techniques, allowing for better attribution of predicted subsidence to underlying physical processes. Finally, transfer learning and domain adaptation strategies will be investigated to facilitate the application of trained models to new geographic areas with differing geologic and anthropogenic characteristics

Acknowledgment

The authors extend their appreciation to the Deanship of Scientific Research at Northern Border University, Arar, KSA for funding this research work through the project number “NBU-FFMRA-2025-2441-01”.

References

[1] C. Jia, X. Yang, J. Wu, P. Ding, and C. Bian, "Monitoring analysis and numerical simulation of the land subsidence in linear engineering areas," KSCE Journal of Civil Engineering, vol. 25, no. 7, Jul. 2021, pp. 2674–2689.

[2] X. Liu, Y. Zhang, J. Zhang, T. Yang, P. Jia, and R. Guo, "Modelling surface subsidence of coal mines using a bonded block numerical method," Geomatics, Natural Hazards and Risk, vol. 15, no. 1, 2024, Art. no. 2336017.

[3] R. Malaoui, M. R. Soltani, A. Djellali, A. Soukeur, and R. Kechiched, "Geotechnical characterization of phosphate mining waste materials for use in pavement construction," Engineering, Technology & Applied Science Research, vol. 13, no. 1, Feb. 2023, pp. 10005–10013.

[4] E. Rafiei Sardooi, H. R. Pourghasemi, A. Azareh, F. Soleimani Sardoo, and J. J. Clague, "Comparison of statistical and machine learning approaches in land subsidence modelling," Geocarto International, vol. 37, no. 21, 2022, pp. 6165–6185.

[5] L. Gazzola et al., "A novel methodological approach for land subsidence prediction through data assimilation techniques," Computational Geosciences, vol. 25, 2021, pp. 1731–1750.

[6] R. Wang et al., "A novel method of monitoring surface subsidence law based on probability integral model combined with active and passive remote sensing data," Remote Sensing, vol. 14, no. 2, Jan. 2022, Art. no. 299.

[7] D. M. Zhang, X. L. Zhang, and W. W. Du, "Discrete element method based investigation on displacement and bearing characteristics of pile foundation under seepage erosion," Rock and Soil Mechanics, vol. 45, no. 4, Apr. 2024, Art. no. 8.

[8] C. Y. Ku and C. Y. Liu, "Modeling of land subsidence using GIS-based artificial neural network in Yunlin County, Taiwan," Scientific Reports, vol. 13, no. 1, Mar. 2023, Art. no. 4090.

[9] A. Aditiya and T. Ito, "Present-day land subsidence over Semarang revealed by time series InSAR new small baseline subset technique," International Journal of Applied Earth Observation and Geoinformation, vol. 125, 2023, Art. no. 103579.

[10] W. L. Hakim et al., "InSAR time-series analysis and susceptibility mapping for land subsidence in Semarang, Indonesia using convolutional neural network and support vector regression," Remote Sensing of Environment, vol. 287, 2023, Art. no. 113453.

[11] G. Wang et al., "Coastal subsidence detection and characterization caused by brine mining over the Yellow River Delta using time series InSAR and PCA," International Journal of Applied Earth Observation and Geoinformation, vol. 114, 2022, Art. no. 103077.

[12] T. Y. Kwak, S. Hong, J. H. Lee, and S. I. Woo, "Analysis of the limitations of the existing subsidence prediction method based on the subsidence measurement data and suggestions for improvement method through weighted nonlinear regression analysis," Journal of the Korean Geotechnical Society, vol. 38, no. 12, 2022, pp. 103–112.

[13] J. Wang et al., "Control and prevent land subsidence caused by foundation pit dewatering in a coastal lowland megacity: indicator definition, numerical simulation, and regression analysis," Environmental Earth Sciences, vol. 82, no. 2, Feb. 2023, Art. no. 66.

[14] J. Li, Z. He, C. Piao, W. Chi, and Y. Lu, "Research on subsidence prediction method of water-conducting fracture zone of overlying strata in coal mine based on grey theory model," Water, vol. 15, no. 23, Dec. 2023, Art. no. 4177.

[15] D. Yuan et al., "Application of optimized grey-Markov model to land subsidence monitoring with InSAR," IEEE Access, vol. 10, 2022, pp. 96720–96730.

[16] B. Li, N. Liu, and W. Wang, "Coupling model based on grey relational analysis and stepwise discriminant analysis for subsidence discrimination of foundation in soft clay areas," International Journal of Computational Science and Engineering, vol. 24, no. 1, 2021, pp. 55–63.

[17] S. Mehrnoor et al., "Land subsidence hazard assessment based on novel hybrid approach: BWM, weighted overlay index (WOI), and support vector machine (SVM)," Natural Hazards, vol. 115, no. 3, 2023, pp. 1997–2030.

[18] L. Wang et al., "Automatic-detection method for mining subsidence basins based on InSAR and CNN-AFSA-SVM," Sustainability, vol. 14, no. 21, Nov. 2022, Art. no. 13898.

[19] D. Zhou, X. Zuo, and Z. Zhao, "Constructing a large-scale urban land subsidence prediction method based on neural network algorithm from the perspective of multiple factors," Remote Sensing, vol. 14, no. 8, Apr. 2022, Art. no. 1803.

[20] S. Kumar, D. Kumar, P. K. Donta, and T. Amgoth, "Land subsidence prediction using recurrent neural networks," Stochastic Environmental Research and Risk Assessment, vol. 36, no. 2, 2022, pp. 373–388.

[21] Q. Qi et al., "Spatial prediction of soil organic carbon in coal mining subsidence areas based on RBF neural network," International Journal of Coal Science & Technology, vol. 10, no. 1, 2023, Art. no. 30.